

Skyrmion Phase and Non-Fermi Liquid Behavior in Nonsymmorphic Magnetic Weyl Semimetal

Xi Luo¹ and Yue Yu^{2,*}

¹College of Science, University of Shanghai for Science and Technology, Shanghai 200093, China

²Department of Physics, Fudan University, Shanghai 200433, China

(Dated: February 26, 2026)

We investigate the interplay between complex magnetic orders and topological electronic states in nonsymmorphic magnetic Weyl semimetals on the ReAlX family (Re is a rare earth element and X is Si or Ge). We construct a lattice model incorporating conduction Weyl fermions coupled to localized magnetic moments via Kondo interaction. By considering a multi- \mathbf{Q} cycloid magnetic configuration, which can evolve into a Skyrmion lattice under an in-plane Zeeman field, we analyze its profound impact on the band structure through magnetic Brillouin zone and band-folding. Using the Kubo formula, we calculate the conductivity tensor and examine the transport properties in the clean limit. Our results reveal that the Skyrmion lattice induces significant changes in electrical and Hall conductivities. Furthermore, the temperature-dependent resistivity deviates from the standard Fermi-liquid behavior ($\rho_{xx} \sim T^2$), showing a power-law scaling ($\rho_{xx} \sim T^\alpha$ with α between 3 and 5), indicative of non-Fermi liquid behavior. This work provides a theoretical framework connecting multi- \mathbf{Q} magnetic textures, Skyrmion physics, and anomalous transport in topological semimetals.

Introduction—A recently discovered class of non-collinear magnetic Weyl semimetals, ReAlX (Re is a rare earth element and X is Si or Ge) family of materials, has emerged as an ideal platform for exploring the interplay of topological electronic states and strongly correlated physics, owing to their simultaneous possession of topological electronic bands and rich magnetic orders [1–7]. In these Weyl semimetal candidates, both time-reversal and inversion symmetries are broken, therefore, non-zero Heisenberg, Dzyaloshinskii-Moriya (DM), and Kitaev-Ising interactions are allowed by the Ruderman-Kittel-Kasuya-Yosida (RKKY) interactions mediated by the Weyl fermion [8–12]. Meanwhile, the localized 4f electrons of the rare-earth elements introduce complex magnetic interactions, giving rise to a variety of novel magnetic structures such as helical, cycloidal, and even Skyrmion lattice orders [5, 7]. Of particular interest is the series of significant anomalous transport phenomena experimentally observed in this family. For instance, a large topological Hall effect (THE) has been discovered in the "A-phase" of SmAlSi [5], nearly perfect multi- \mathbf{Q} spin cycloid textures have been observed in GdAlSi [7], and longitudinal resistivity scaling of $\sim T^3$ near 10K, deviating from conventional Fermi liquid theory ($\sim T^2$) or the simple linear behavior of Weyl fermions ($\sim T$) [13], has been reported in PrAlGe and LaAlGe [2, 4]. The non-Fermi liquid behavior has also been reported in the Skyrmion lattice phase of MnSi [14].

The physical origin of these anomalous transport behaviors is widely believed to be intimately linked to the complex magnetic orders, topological electronic states, and the strong interaction between them within these materials. On one hand, non-collinear magnetic structures (such as Skyrmions) formed by localized magnetic

moments generate a real-space Berry curvature, which acts as an effective magnetic field on conduction electrons, i.e., the THE [15, 16]. On the other hand, the interaction between conduction electrons (here, the Weyl fermions) and localized moments is bidirectional. Localized moments indirectly influence conduction electrons via the RKKY interaction, while the itinerant nature of Weyl fermions, in turn, modulates this interaction [8–12]. This can lead to long-range and anisotropic magnetic exchange, potentially stabilizing complex multi- \mathbf{Q} magnetic orders. Furthermore, direct interactions such as the on-site Kondo coupling further entangle the magnetic order with the electronic band structure, potentially inducing band folding, gap opening, or shifting of Weyl nodes, thereby fundamentally altering the Fermi surface topology and low-energy excitation spectrum of the system [17, 18].

Despite the growing body of experimental observations, a unified and clear theoretical picture is still lacking for how specific magnetic structures (such as the Skyrmion lattice evolving from multi- \mathbf{Q} cycloid orders) quantitatively affect the transport of Weyl fermions and lead to non-Fermi-liquid behavior in the ReAlX family. Understanding this mechanism tangling the topologies between Weyl fermion (in momentum space) and the magnetic order (in real space) is not only key to unraveling the exotic quantum phenomena in these materials but also holds significant implications for the future design of novel spintronic and topological electronic devices based on topological magnetic textures, such as low-power magnetic memory and topological Hall sensors [19–23].

Motivated by this, the present work aims to establish an effective microscopic theoretical model to systematically investigate the interaction between Weyl fermions and a Skyrmion lattice composed of multi- \mathbf{Q} cycloid magnetic orders in ReAlX materials, and its impact on transport properties. We first construct an effective lattice Hamiltonian incorporating Kondo coupling, an-

* Correspondence to: yuyue@fudan.edu.cn

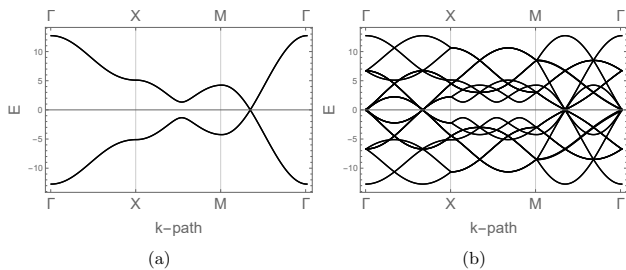


FIG. 1. (color online) The band structures of $k_z = 0$ plane of (a) H_0 and (b) H . $m_1 = m_2 = 3$, $u_1 = v_2 = 4$, $v_1 = u_2 = 2$, $v_0 = 1$, $a = b = 0$, and $K = 0.2$. In (a), the Weyl nodes are located near $(\pm \frac{2\pi}{3}, \pm \frac{2\pi}{3}, 0)$. In (b), there are extra Weyl nodes emerge near the Γ point, $(\pm \frac{2\pi}{3}, 0, 0)$, and $(0, \pm \frac{2\pi}{3}, 0)$ due to the band folding caused by the multi- \mathbf{Q} magnetic order \mathbf{M} (3).

alyzing the magnetic Brillouin zone folding induced by the Skyrmion background and its reshaping of the band structure. Subsequently, by calculating the conductivity tensor via the Kubo formula in the clean limit, we theoretically reproduce the correlation between the sign change of the topological Hall resistivity and a non-trivial Skyrmion number. Furthermore, we elucidate how the temperature scaling of the longitudinal resistivity evolves into a non-Fermi-liquid behavior between T^3 and T^5 under the influence of magnetic order, providing a theoretical explanation for relevant experimental observations. This study offers a new perspective for understanding the entanglement between magnetic order and topological transport in magnetic topological materials.

Lattice model—In the ReAlX-family materials, the nearly commensurate magnetic order couples the Weyl nodes located in the $k_z = 0$ plane [5, 7], which can be described by the following lattice model [1],

$$\begin{aligned}
 H_0 = & (m_1 + u_1 \cos k_x + v_1 \cos k_y) \chi_0 \sigma_1 + t_0 \sin k_z \chi_3 \sigma_2 \\
 & + (m_2 + u_2 \cos k_x + v_2 \cos k_y) \chi_0 \sigma_3 \\
 & + a(\chi_3 \sigma_1 - \chi_3 \sigma_3) + b \chi_3 \sigma_2,
 \end{aligned} \quad (1)$$

where σ_i and χ_i are Pauli matrices acting on spin and orbital indices, respectively. To compare with the experiments [5, 7], we choose $m_1 = m_2 = 3$, $u_1 = v_2 = 4$, $v_1 = u_2 = 2$, and $v_0 = 1$, then there are eight massless Dirac points located at $(\pm \frac{2\pi}{3}, \pm \frac{2\pi}{3}, 0)$ and $(\pm \frac{2\pi}{3}, \pm \frac{2\pi}{3}, \pi)$ when $a = b = 0$ (see Fig. 1a). a and b terms are perturbations that keep C_4 rotation symmetry. For $a \neq 0$, a Dirac node is split into two Weyl nodes with opposite chiralities. For $b \neq 0$, inversion and time-reversal symmetries are broken. This moves the Weyl nodes away from $k_z = 0, \pm\pi$ planes.

Due to the breaking of inversion and time-reversal symmetries in the ReAlX-family materials, there can be non-zero Heisenberg, DM, and Kitaev-Ising interactions between the strong magnetic moments of the f electrons of the rare-earth elements and complicated magnetic configurations, such as (anti-)ferromagnet, canted, helical,

cycloidal, spiral, and Skyrmion may exist [5]. These interactions can be induced through the RKKY interactions mediated by the Weyl fermions [8–12]. In turn, these non-trivial magnetic configurations can drastically change the physical properties of the Weyl fermions, such as the anomalous non-Fermi liquid transport properties observed in ReAlX-family materials [2–4, 6] while a clear theoretical understanding remains lacking.

To further investigate the interplay between the magnetic configurations and the conducting Weyl fermions, we consider the following effective Hamiltonian,

$$H = H_0 + H_K, \quad H_K = \sum_i K \mathbf{s}_i \cdot \mathbf{M}_i, \quad (2)$$

where i is the lattice site, K is the on-site Kondo coupling between the conduction Weyl fermion and the magnetic moment of the rare-earth elements [17, 18]. \mathbf{s}_i is the spin of the Weyl fermion and \mathbf{M}_i is the magnetic configuration. In the following, we use an adiabatic approximation when solving the conduction electron problem, i.e., the conduction Weyl fermions are assumed to be fast-moving with respect to the fluctuations of magnetic configuration \mathbf{M} and \mathbf{M} is treated as a background.

In principle, many complicated magnetic configurations can emerge due to the competitions among Heisenberg, DM, and Kitaev-Ising interactions, let alone the influence of the conducting Weyl fermions. Here, we focus on the Skyrmion configuration and the correlation physics between the Skyrmion lattice and the Weyl fermions. More detailed (finite-temperature) phase diagrams with different types of magnetic orders can be obtained by comparing the Gibbs free energies and will be present in future works.

Multi- \mathbf{Q} magnetic order, Skyrmion lattice and band structures—The Skyrmion phase (A-phase) and THE have been observed in helimagnets such as MnSi and Gd₃Ru₄Al₁ [15, 16]. In ReAlX-family, a similar A-phase and THE are reported in SmAlSi [5]. Furthermore, perfectly harmonic spin cycloid and multi- \mathbf{Q} textures with nearly nesting $\mathbf{Q}_1 = 2\pi(\frac{2}{3}, -\frac{2}{3}, 0)$ and $\mathbf{Q}_3 = 2\pi(\frac{2}{3}, \frac{2}{3}, 0)$ between the Weyl nodes are reported in GdAlSi [7]. Since the Skyrmion lattice can be obtained from a linear composition of the helical/cycloid magnetic configurations with multi- \mathbf{Q} structures [24], it is reasonable to assume the emergence of A-phase in ReAlX-family is related to the multi- \mathbf{Q} behavior of the magnetic configurations. Furthermore, the A-phase in SmAlSi emerges within a regime with finite temperature and in plane external magnetic field [5], which suggests that the Skyrmion lattice is composed by multi- \mathbf{Q} cycloid configurations instead of helical ones. The reason is that if the Skyrmion lattice is composed by multi- \mathbf{Q} helical configurations, then the A-phase should emerge with a finite external magnetic field perpendicular to the \mathbf{Q}_1 - \mathbf{Q}_2 plane, which is in conflict with the experimental observations.

Inspired by the experimental observations [5, 7], we

consider the following magnetic configuration

$$\begin{aligned} \mathbf{M} = & (\cos(\mathbf{r} \cdot \mathbf{Q}_2) - \cos(\mathbf{r} \cdot \mathbf{Q}_1), \\ & \sin(\mathbf{r} \cdot \mathbf{Q}_2) + \sin(\mathbf{r} \cdot \mathbf{Q}_1), \sin(\mathbf{r} \cdot \mathbf{Q}_2) - \sin(\mathbf{r} \cdot \mathbf{Q}_1)), \end{aligned} \quad (3)$$

which is the combination of two cycloid magnetic configurations along \mathbf{Q}_1 and \mathbf{Q}_2 . The Skyrmion charge is defined by [24]

$$N_s = \int d^2\mathbf{r} \frac{1}{4\pi} \hat{\mathbf{n}} \cdot (\partial_x \hat{\mathbf{n}} \times \partial_y \hat{\mathbf{n}}), \quad (4)$$

where $\hat{\mathbf{n}} = \mathbf{M}/|\mathbf{M}|$. To obtain a nonzero Skyrmion charge, an external in plane magnetic field is necessary. Therefore, we add a Zeeman term H_λ into the system Hamiltonian as the effect induced by the external magnetic field,

$$H_\lambda = \sum_{a=1}^3 \lambda_a \sigma_a, \quad (5)$$

where λ_a is the Zeeman's strength along the a -direction. One can effectively add a term $\frac{2}{K}(\lambda_1, \lambda_2, \lambda_3)$ into the magnetic configuration \mathbf{M} (3) when combining H_K and H_λ together.

We plot a typical Skyrmion lattice in Fig. 2. By applying a in-plane Zeeman field along the x -direction, there are two Skyrmions within a magnetic unit cell. By choosing $K = 0.2$, $\lambda_1 = 0.1$, and $\lambda_2 = \lambda_3 = 0$ (see Fig. 2a and Fig. 2b), which is consistent with the Skyrmion number $N_s = -2$ within a magnetic unit cell (see Fig. 2d). Without the in-plane Zeeman field, the Skyrmion number is zero when applying Zeeman field in the perpendicular direction alone, which is consistent with the condition for the emergence of A-phase observed in the experiments [5].

The free Weyl semimetal band structure changes drastically by considering the influence of the Skyrmion lattice through the Kondo coupling H_K . Especially, the Skyrmion lattice will introduce a magnetic Brillouin zone [18]. Denote

$$|\Psi\rangle = \sum_{i,j=1}^3 \psi_{i,j} c^\dagger(k_x^0 + Qi, k_y^0 + Qj, k_z)|0\rangle, \quad (6)$$

where $Q = 4\pi/3$ is the norm of the nesting vectors \mathbf{Q}_1 and \mathbf{Q}_2 , $-\frac{\pi}{3} \leq k_x^0, k_y^0 \leq \frac{\pi}{3}$, and $-\pi \leq k_z \leq \pi$. Then, the Schrödinger equation $H|\Psi\rangle = E|\Psi\rangle$ reduces to the Harper equation [18, 25–27] (for more details, see Appendix A).

We plot the band structure in Fig. 2b with $K = 0.2$. There are extra Weyl nodes emerging due to the band folding caused by the multi- \mathbf{Q} magnetic order \mathbf{M} . With finite in-plane Zeeman field, The magnetic order \mathbf{M} can evolve into a Skyrmion lattice (see Fig. 2d), and the Weyl node slightly moves away from its original point for a small Zeeman field. Therefore, the physical properties can change drastically due to the band folding.

Conductivity and non-Fermi liquid behavior— Experimentally, the transport behaviors of ReAlX-family materials are anomalous and have attract lots of research attentions. For instance, large THE is observed in the A-phase of SmAlSi [5], the magnetoresistance change from positive to negative near 12.8K in CeAlGe [6], the behavior of electric resistance ρ_{xx} changes drastically in NdAlSi when the background magnetic configuration changes from helical magnet to ferromagnet [3], and $\rho_{xx} \sim T^3$ in PrAlGe and LaAlGe near $T \sim 10K$, which deviates from T linear behavior of Weyl fermion, or the T^2 behavior of Fermi liquids, or T^5 behavior of the electron-phonon interaction, and is believed to be caused by $s-d$ inter-band scattering [2, 4, 13]. Many of the above mentioned anomalous phenomena lack a systematic and theoretic understanding. Here we study the conductivity σ_{ab} of the lattice model in the clean limit by the Kubo formula, we find that there is a peak at the phase boundary between lattice with a non-trivial Skyrmion number and a trivial one, the temperature dependence of the longitudinal resistance shows a non-Fermi liquid behavior, and the coupling to the multi- \mathbf{Q} cycloid magnetic order drives the system into a bad-metal regime. A more detailed study on the effects of disorder and interactions will be present in future works.

The Kubo formula reads,

$$\sigma_{ab} = \frac{ie^2}{h} \int_{BZ} \frac{d^3k}{(2\pi)^3} \sum_{m,n} \frac{f_{nk} - f_{mk}}{E_{nk} - E_{mk}} \frac{\langle nk|v_a|nk\rangle \langle nk|v_b|nk\rangle}{E_{mk} - E_{nk} + i\eta}, \quad (7)$$

where a, b is the spacial indices, E_{nk} is the n th band energy of the state $|nk\rangle$ with momentum \mathbf{k} , f_{nk} is the Fermi-Dirac distribution of E_{nk} , $v_a = \frac{1}{\hbar} \frac{\partial H}{\partial k_a}$, and $\eta \rightarrow 0^+$. We plot the corresponding conductance in Fig. 3. We choose $\eta = 0.0001$ and use the classical Monte-Carlo method to numerically evaluate the Kubo formula with the number of the samples $N = 90000$ and the random seed being 12345. The results for the total Hamiltonian with nesting multi- \mathbf{Q} cycloid magnetic configuration is divided by 9 due to the band-folding. In SmAlSi, the hopping constant $t \sim 100meV$, and the energy of Weyl node is about $-20meV$ [5], therefore, to simulate the situation in SmAlSi, we choose $a = 0.1$, $b = 0.2$ and the fermi level $E_f = 0$ in H_0 (1), which corresponds to $-20meV$ for the Weyl node energy after setting the hopping constant $t = 1$.

$\lambda_x = 0.2$ is the phase boundary between the non-trivial Skyrmion number and the trivial one. From Fig. 3a and Fig. 3b, we notice that there are peaks in both σ_{xx} and σ_{xy} at $\lambda_x = 0.2$ which indicates a phase transition. And for $\lambda_x < 0.2$, the σ_{xy} is in general above zero while for $\lambda_x > 0.2$, σ_{xy} quickly drops below zero.

The conductivity σ and the electric resistance ρ is related by

$$\sigma_{xx} = \frac{\rho_{xx}}{\rho_{xx}^2 + \rho_{xy}^2}, \quad \sigma_{xy} = \frac{-\rho_{xy}}{\rho_{xx}^2 + \rho_{xy}^2}. \quad (8)$$

We fit the resistance ρ_{xx} with temperature by the rela-

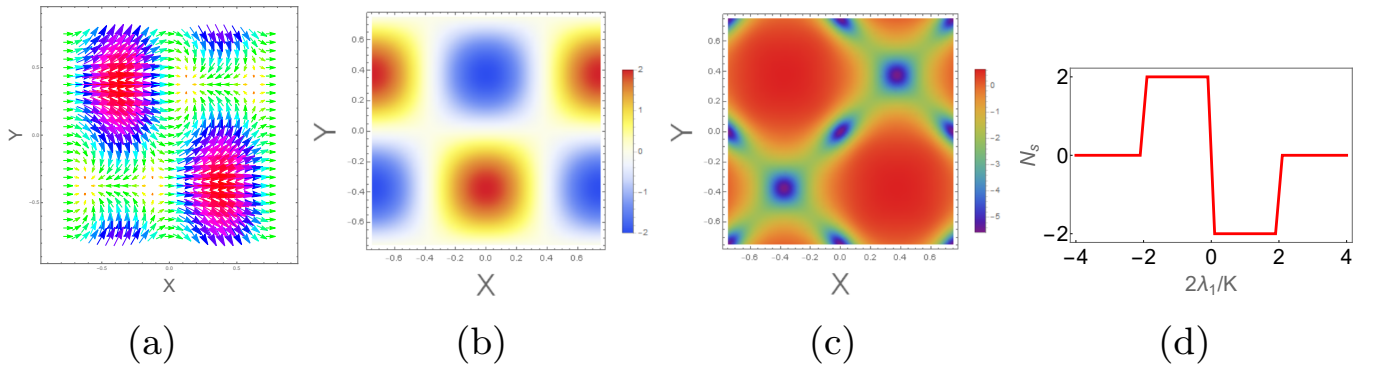


FIG. 2. (color online) The distributions of (a) the (M_1, M_2) and (b) the M_3 components of magnetization \mathbf{M} in a magnetic unit cell. (c) The density distribution of Skyrion number N_s in a magnetic unit cell. In (a), (b), and (c), the Kondo coupling $K = 0.2$ and the Zeeman strength $\lambda_1 = 0.1$, $\lambda_2 = \lambda_3 = 0$. (d) The dependence of the Skyrion number N_s with respect to the in-plane Zeeman field and Kondo coupling in a magnetic unit cell.

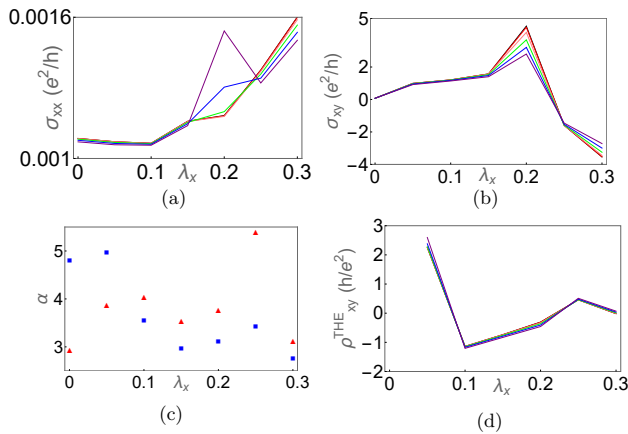


FIG. 3. (color online) We plot the conductivity tensor in (a) and (b), and the resistance of THE in (d). The black, red, pink, green, blue, purple lines correspond to $T = 5K, 10K, 15K, 20K, 25K$ and $30K$ respectively. (c) We plot the fitted α versus λ_x with blue square and red triangle stands for the free Hamiltonian (1) and the total Hamiltonian H with Kondo interaction (2). In all mini-figures, the external in-plane magnetic field is applied along x -direction.

tion $\rho_{xx} = a + bT^\alpha$, where a and b are constants and the fitted α are shown in Fig. 3c. Without external magnetic field, $\alpha \sim 4.9$ for the free model H_0 and $\alpha \sim 2.9$ after considering the nesting multi- \mathbf{Q} cycloid magnetic configuration, and this case is consistent with the experimental observations in PrAlGe and LaAlGe [2, 4]. After applying the in-plane magnetic field, α lies between 3 – 5 for both the free Hamiltonian H_0 (1) and with the Kondo interaction H (2), which are all deviates from the Fermi liquid behavior $\rho_{xx} \sim T^2$.

In Fig. 3d, we plot the resistance of THE ρ_{xy}^{THE} by subtracting the contribution of anomalous Hall effect ρ_{xy}^A of the free Hamiltonian H_0 (1) from the total Hall resistance ρ_{xy} . We find that the large ρ_{xy}^{THE} fluctuates between positive and negative which indicates the influ-

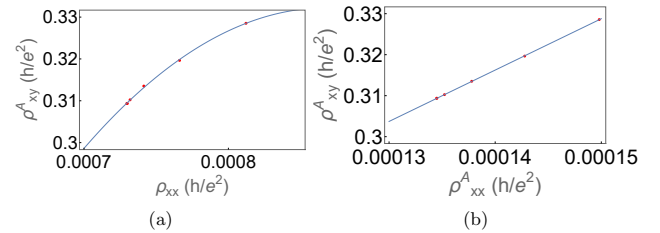


FIG. 4. (color online) The scaling behavior of anomalous Hall resistance versus the electric resistance. (a) ρ_{xy}^A vs. ρ_{xx} , and (b) ρ_{xy}^A vs. ρ_{xx}^A . We choose $\lambda_x = 0.1$ in (a) and (b), and the data is obtained from different temperatures. ρ_{xy}^A and ρ_{xx}^A is obtained from the free Hamiltonian H_0 (1) while ρ_{xx} is from the total Hamiltonian H (2).

ence of Skyrion lattice on the transport of the Weyl fermions. Furthermore, then $\lambda_x = 0.3$, $\rho_{xy}^{THE} \sim 0$ which is consistent with the Skyrion number $N_s = 0$ where ρ_{xy}^{THE} is proportional to the Skyrion number [28]. A more detailed study on the motion of semiclassical wave package of Weyl fermion under the effect of the Berry phase of Skyrion lattice will be present in future works [29].

Furthermore, we draw the scaling behavior of anomalous Hall resistance ρ_{xy}^A versus the longitudinal resistance ρ_{xx} in Fig. 4. The anomalous Hall resistance ρ_{xy}^A is obtained from the free Hamiltonian H_0 (1). We find that the nesting multi- \mathbf{Q} cycloid magnetic configuration turns the Weyl semimetal into a bad-metal regime for $\rho_{xy}^A \sim \rho_{xx}^2$ (see Fig. 4a) while the free system is in a high conductivity regime for $\rho_{xy}^A \sim \rho_{xx}^A$ where ρ_{xx}^A is the longitudinal resistance for the free Hamiltonian H_0 (1) [30].

Conclusions—We have theoretically demonstrated that in nonsymmorphic magnetic Weyl semimetals such as those in the ReAlX family, the multi- \mathbf{Q} cycloid magnetic orders, which can form a Skyrion lattice, significantly alters the electronic and transport properties.

The Skyrmion lattice, stabilized by an in-plane Zeeman field, introduces magnetic Brillouin zone, leading to the emergence of additional Weyl nodes and modified band-folding structures. The transverse Hall conductivity shows a distinct response near the phase boundary of non-trivial Skyrmion number, corroborating the intimate link between topological Hall effect and Skyrmion topology. The temperature scaling of resistivity deviates from conventional Fermi-liquid theory, exhibiting a non-Fermi liquid power-law behavior, consistent with experimental observations in related materials. The scaling relation between anomalous Hall resistivity and longitudinal resistivity reveals that the magnetic order drives the system into a bad-metal regime. These results establish a coherent picture of how Skyrmion textures interact with Weyl fermions, leading to anomalous transport signatures and non-Fermi liquid behavior. Future work should address the roles of disorder, interactions, and the semiclassical dynamics of wave packets in the Berry phase landscape of Skyrmion lattices. This study advances the under-

standing of correlated topological phases and provides a foundation for exploring exotic quantum phenomena and future design of novel spintronic devices in nonsymmorphic magnetic Weyl materials.

ACKNOWLEDGMENTS

The authors thank Long Liang for useful discussions. This work is supported by the National Natural Science Foundation of China with Grant No. 12174067.

DATA AVAILABILITY

The data that support the findings of this article are not publicly available. The data are available from the authors upon reasonable request.

-
- [1] G. Chang, B. Singh, S.-Y. Xu, G. Bian, S.-M. Huang *et al.*, Theoretical prediction of magnetic and noncentrosymmetric Weyl fermion semimetal states in the R-Al-X family of compounds (R=rare earth, Al=aluminium, X=Si, Ge), *Phys. Rev. B* **97**, 041104 (2018).
- [2] D. Destraz, L. Das, S. S. Tsirkin, Y. Xu, T. Neupert, J. Chang, A. Schilling, A. G. Grushin, J. Kohlbrecher, L. Keller, P. Pupal, E. Pomjakushina and J. S. White, Magnetism and anomalous transport in the Weyl semimetal PrAlGe: possible route to axial gauge fields, *npj Quantum Materials* **5**, 5 (2020).
- [3] J. Gaudet, H.-Y. Yang, S. Baidya, B. Lu, G. Xu, Y. Zhao, J. A. Rodriguez-Rivera, C. M. Hoffmann, D. E. Graf, D. H. Torchinsky, P. Nikolić, D. Vanderbilt, F. Tafti, and C. L. Broholm, Weyl-mediated helical magnetism in NdAlSi, *Nat. Mater.* **20**, 1650 (2021).
- [4] Niraj Bhattarai, Andrew W. Forbes, Christopher Gassen, Raghad S. H. Saqat, Ian L. Pegg, and J. Philip, Experimental study of transport properties of Weyl semimetal LaAlGe thin films grown by molecular beam epitaxy, *J. Vac. Sci. Technol. A* **39**, 063407 (2021).
- [5] X. Yao, J. Gaudet, R. Verma, D. E. Graf, H.-Y. Yang *et al.*, Large Topological Hall Effect and Spiral Magnetic Order in the Weyl Semimetal SmAlSi, *Phys. Rev. X* **13**, 011035 (2023).
- [6] N. C. Drucker, T. Nguyen, F. Han, P. Siriviboon, X. Luo, N. Andrejevic, Z. Zhu, G. Bednik, Q. T. Nguyen, Z. Chen, L. K. Nguyen, T. Liu, T. J. Williams, M. B. Stone, A. I. Kolesnikov, S. Chi, J. Fernandez-Baca, C. S. Nelson, A. Alatas, T. Hogan, A. A. Puretzky, S. Huang, Y. Yu, and Mingda Li, Topology stabilized fluctuations in a magnetic nodal semimetal, *Nat. Commun.* **14**, 5182 (2023).
- [7] R. Nakano, R. Yamada, J. Bouaziz, M. Colling, M. Gen *et al.*, Perfectly harmonic spin cycloid and multi-Q textures in the Weyl semimetal GdAlSi, arXiv: 2503.14768.
- [8] H.-R. Chang, J. Zhou, S.-X. Wang, W.-Y. Shan, and D. Xiao, RKKY interaction of magnetic impurities in Dirac and Weyl semimetals, *Phys. Rev. B* **92**, 241103(R) (2015).
- [9] M. V. Hosseini and M. Askari, Ruderman-Kittel-Kasuya-Yosida interaction in Weyl semimetals, *Phys. Rev. B* **92**, 224435 (2015).
- [10] J.-H. Sun, D.-H. Xu, F.-C. Zhang, and Y. Zhou, Magnetic impurity in a Weyl semimetal, *Phys. Rev. B* **92**, 195124 (2015).
- [11] S.-X. Wang, H.-R. Chang, and J. Zhou, RKKY interaction in three-dimensional electron gases with linear spin-orbit coupling, *Phys. Rev. B* **96**, 115204 (2017).
- [12] M. Zhou, H.-R. Chang, L. Yang, and L. Liang, Weyl-mediated Ruderman-Kittel-Kasuya-Yosida interaction revisited: Imaginary-time formalism and finite temperature effects, *Phys. Rev. B* **112**, 054449 (2025).
- [13] P. Hosur, S. A. Parameswaran, and A. Vishwanath, Charge Transport in Weyl Semimetals, *Phys. Rev. Lett.* **108**, 046602 (2012).
- [14] R. Ritz, M. Halder, M. Wagner, C. Franz, A. Bauer, and C. Pfleiderer, Formation of a topological non-Fermi liquid in MnSi, *Nature* **497**, 231 (2013).
- [15] A. Neubauer, C. Pfleiderer, B. Binz, A. Rosch, R. Ritz, P. G. Niklowitz, and P. Böni, Topological Hall Effect in the A Phase of MnSi, *Phys. Rev. Lett.* **102**, 186602 (2009).
- [16] M. Hirschberger, T. Nakajima, S. Gao, L. Peng, A. Kikkawa, T. Kurumaji, M. Kriener, Y. Yamasaki, H. Sagayama, H. Nakao, K. Ohishi, K. Kakurai, Y. Taguchi, X. Yu, T.-h. Arima, and Y. Tokura, Skyrmion Phase and Competing Magnetic Orders on a Breathing Kagomé Lattice, *Nat. Commun.* **10**, 5831 (2019).
- [17] A. K. Mitchell and L. Fritz, Kondo effect in three-dimensional Dirac and Weyl systems, *Phys. Rev. B* **92**, 121109(R) (2015).
- [18] X. Luo, Y.-G. Chen, Y.-M. Zhan, and Y. Yu, Correlated helimagnetic configuration in a nonsymmorphic magnetic nodal semimetal, *Phys. Rev. B* **112**, 115116 (2025).
- [19] B. A. Bernevig, C. Felser, and H. Beidenkopf, Progress and prospects in magnetic topological materials, *Nature*

$$\sin(Q(x+y)) \sim \frac{1}{2i} \begin{bmatrix} 0 & 0 & 0 & 0 & 1 & 0 & 0 & 0 & -1 \\ 0 & 0 & 0 & 0 & 0 & 0 & 0 & 0 & 0 \\ 0 & 0 & 0 & 0 & 0 & 0 & 0 & 0 & 0 \\ 0 & 0 & 0 & 0 & 0 & 0 & 0 & 0 & 0 \\ -1 & 0 & 0 & 0 & 0 & 0 & 0 & 0 & 1 \\ 0 & 0 & 0 & 0 & 0 & 0 & 0 & 0 & 0 \\ 0 & 0 & 0 & 0 & 0 & 0 & 0 & 0 & 0 \\ 0 & 0 & 0 & 0 & 0 & 0 & 0 & 0 & 0 \\ 1 & 0 & 0 & 0 & -1 & 0 & 0 & 0 & 0 \end{bmatrix}, \quad \sin(Q(x-y)) \sim \frac{1}{2i} \begin{bmatrix} 0 & 0 & 0 & 0 & 0 & 1 & 0 & -1 & 0 \\ 0 & 0 & 0 & 0 & 0 & 0 & 0 & 0 & 0 \\ 0 & 0 & 0 & 0 & 0 & 0 & 0 & 0 & 0 \\ 0 & 0 & 0 & 0 & 0 & 0 & 0 & 0 & 0 \\ 0 & 0 & 0 & 0 & 0 & 0 & 0 & 0 & 0 \\ 0 & 0 & 0 & 0 & 0 & 0 & 0 & 0 & 0 \\ -1 & 0 & 0 & 0 & 0 & 0 & 0 & 1 & 0 \\ 0 & 0 & 0 & 0 & 0 & 0 & 0 & 0 & 0 \\ 1 & 0 & 0 & 0 & 0 & -1 & 0 & 0 & 0 \\ 0 & 0 & 0 & 0 & 0 & 0 & 0 & 0 & 0 \end{bmatrix}, \quad (\text{A7})$$

$$\sin k_x \sim \begin{bmatrix} \sin k_x & 0 & 0 & 0 & 0 & 0 & 0 & 0 & 0 \\ 0 & \sin k_x & 0 & 0 & 0 & 0 & 0 & 0 & 0 \\ 0 & 0 & \sin k_x & 0 & 0 & 0 & 0 & 0 & 0 \\ 0 & 0 & 0 & \sin(k_x + Q) & 0 & 0 & 0 & 0 & 0 \\ 0 & 0 & 0 & 0 & \sin(k_x + Q) & 0 & 0 & 0 & 0 \\ 0 & 0 & 0 & 0 & 0 & \sin(k_x + Q) & 0 & 0 & 0 \\ 0 & 0 & 0 & 0 & 0 & 0 & \sin(k_x + 2Q) & 0 & 0 \\ 0 & 0 & 0 & 0 & 0 & 0 & 0 & \sin(k_x + Q) & 0 \\ 0 & 0 & 0 & 0 & 0 & 0 & 0 & 0 & \sin(k_x + 2Q) \end{bmatrix}, \quad (\text{A8})$$

$$\sin k_y \sim \begin{bmatrix} \sin k_y & 0 & 0 & 0 & 0 & 0 & 0 & 0 & 0 \\ 0 & \sin(k_y + Q) & 0 & 0 & 0 & 0 & 0 & 0 & 0 \\ 0 & 0 & \sin(k_y + 2Q) & 0 & 0 & 0 & 0 & 0 & 0 \\ 0 & 0 & 0 & \sin k_y & 0 & 0 & 0 & 0 & 0 \\ 0 & 0 & 0 & 0 & \sin(k_y + Q) & 0 & 0 & 0 & 0 \\ 0 & 0 & 0 & 0 & 0 & \sin(k_y + 2Q) & 0 & 0 & 0 \\ 0 & 0 & 0 & 0 & 0 & 0 & \sin k_y & 0 & 0 \\ 0 & 0 & 0 & 0 & 0 & 0 & 0 & \sin(k_y + Q) & 0 \\ 0 & 0 & 0 & 0 & 0 & 0 & 0 & 0 & \sin(k_y + 2Q) \end{bmatrix}. \quad (\text{A9})$$

By diagonalizing the Harper equation, we obtain the band structure of the total Hamiltonian.
